ABraytCSPfuture

Air-Brayton Cycle Concentrated Solar Power future plants via redox oxides-based structured thermochemical heat exchangers / thermal boosters

Deliverable D4.2.

First version of simulation results of redox structures thermochemical expansion

Dissemination Level: Public

WP4 Dual-bed prototype design and solar thermal power plant level system integration scenarios

Date: 31.10.2023

https://www.abraytcspfuture.eu/

This project has received funding from the European Union's Horizon Europe research and innovation programme under grant agreement no 101084569

Disclaimer

The work described in this document has been conducted within the ABraytCSPfuture project that is co-funded by the European Union. Views and opinions expressed herein are however those of the author(s) only and do not necessarily reflect those of the European Union or of the granting authority, European Climate, Infrastructure and Environment Executive Agency (CINEA). Neither the European Union nor the granting authority can be held responsible for them.

Grant Agreement Number: 101084569 Acronym: ABraytCSPfuture				
Full Title	**A**ir-**Brayt**on Cycle **C**oncentrated **S**olar **P**ower **future** plants via redox oxides-based structured thermochemical heat exchangers/thermal boosters			
Call Topic Identifier:	HORIZON-CL5-2021-D3-03			
Funding Scheme	HORIZON EUROPE, RIA – Research and Innovation Actions			
Project start date:	01.11.2022			
Project duration:	48 months			
Project URL	https://www.abraytcspfuture.eu/			
EU Project Officer	Clara Astudillo Llorente			
Project Coordinator	DLR – German Aerospace Center			
Deliverable	D4.2 - First version of simulation results of redox structures thermochemical expansion			
Date of Delivery	Contractual	31.10.2024	Actual	31.10.2024
Nature	Report			
Dissemination Level	Public			
Lead Beneficiary	DLR – German Aerospace Center			

Document History

Version	**Issue Date**	**Change History**	**Authors**	**Organisation**
1.0	28.10.2024	Document drafted	Raisa dos Santos Santana, Daniel Koch	DLR
1.1	31.10.2024	Updated with final partner feedback	Christos Agrafiotis	DLR
1.2	31.10.2024	Final Review	Abhishek Singh	UT

About the Project

ABraytCSPfuture sets forth an innovative, carbon-neutral way for implementing the highly efficient air-Brayton gas turbine power generation cycles into future air-operated Concentrated Solar Power (CSP) plants. Air-Brayton cycles are used in traditional power plants where, however, they involve fossil fuels combustion via pressurised air. *ABraytCSPfuture*'s carbon-neutral approach aims at achieving higher solar-to-electricity efficiencies, vital for the competitiveness of CSP and non-reachable by either PVs or molten salts and thermal oils, increasing in parallel significantly the plants' storage capability. The project will develop and demonstrate a first-of-its-kind compact, dual-bed thermochemical reactor/heat exchanger unit that will transfer heat from a non-pressurised air stream to a pressurised one, while also operating as a thermal booster, raising the temperature of the pressurised stream to the level required for Brayton cycles. Furthermore, the volumetric solar energy storage density of air-operated CSP plants will be significantly increased by rendering their current sensible-only regenerative storage systems to hybrid sensible-thermochemical storage ones within the same storage volume. Both these functionalities will be materialised by thermochemical reactor/heat exchanger units comprised of non-moving, flow-through porous ceramic structures (honeycombs or foams) based on earth-abundant, cost-efficient, non-toxic oxide materials and exploiting reversible reduction/oxidation reactions of such oxides in direct contact with air, accompanied by significant endothermic/exothermic heat effects. The proposed technology is set forth by an interdisciplinary partnership spanning the entire CSP value chain, comprised of leading research centres, universities, innovative SMEs and large enterprises, including ancillary services providers and technology end-users.

Deutsches Zentrum fuer Luft- und Raumfahrt e.V., **DLR**	DE	DLR
Centre for Research & Technology Hellas, **CERTH**	EL	CERTH CENTRE FOR RESEARCH & TECHNOLOGY HELLAS
University of Twente, **UT**	NL	UNIVERSITY OF TWENTE.
Fundación CENER, **CENER**	ES	CENER NATIONAL RENEWABLE ENERGY CENTRE ADItech
Fundación TEKNIKER, **TEKN**	ES	Tekniker
Fraunhofer Gesellschaft zur Foerderung der angewandten Forschung e.V., **FHG (IWKS)**	DE	Fraunhofer IWKS
OPRA Turbines, **OPRA**	NL	Destinus
KRAFTBLOCK GmbH, **KB**	DE	KRAFT BLOCK
LANDSON Emission Technologies A/S, **LET**	DK	landson
COBRA Instalaciones y Servicios S.A., **COBRA**	ES	cobra

Table of Contents

This deliverable is part of a project that has received funding from the European Union's Horizon Europe research and innovation programme under grant agreement no 101084569

Executive Summary

The present document constitutes Deliverable D4.2 "First version of simulation results of redox structures thermochemical expansion" developed within *WP4. Redox oxide materials powder synthesis and application-specific evaluation* of the HORIZON EUROPE 2020 ABraytCSPfuture project. The Deliverable 4.2 provides an overview of the relevance, methodology, activities, and planning associated with the simulation of thermochemical expansion in redox structures. To highlight the importance of this simulation, it is crucial to first examine the significance of evaluating thermal expansion and thermal stresses in redox oxides used in thermochemical energy storage (TCES), while emphasizing the distinctive properties and potential advantages of the specific oxides of interest in the ABraytCSPfuture project, particularly perovskites. Thereafter, a brief review of recent relevant studies is presented, along with the methodology implemented in the project, including the investigation of commercial softwares and custom-developed coding using open-source platforms aimed at Finite Element Method (FEM) simulation, preliminary findings, and next steps.

Changes with respect to the DoA

No changes or deviations from the work plan occurred with respect to this Deliverable *D4.2 First version of simulation results of redox structures thermochemical expansion.*

1. Introduction

Deliverable 4.2 is formulated within the Dual-bed prototype design and solar thermal power plant level system integration scenarios (WP4) and specifically within *Task 4.2. First version of simulation results of redox structures thermochemical expansion,* wherein partners DLR, CERTH and FHG participate. The report summarises the activities and planning relevant to the simulation of thermochemical expansion in redox structures during the period from M18 to M24. To underscore the significance of this type of simulation, it is essential to first discuss the importance of assessing thermal expansion and thermal stresses in redox oxides as applied to thermochemical energy storage (TCES), emphasizing the unique characteristics and potential benefits of the specific oxides of interest in the ABraytCSPfuture project, particularly perovskites. Subsequently, a concise overview of recent pertinent studies is presented, followed by the methodology employed in the project, the initial findings and next steps.

2. Redox oxides applied to TCES

Excess solar energy in air-operated Solar Tower Power Plants can be stored during sunlit operation as sensible heat in porous solid materials, which function as heat exchangers during off-sun periods. The storage capacity of such systems can be enhanced by coating or fabricating the porous heat exchange modules using stoichiometric multivalent metal oxides that undergo reduction/oxidation (redox) reactions, resulting in significant thermal effects (e.g., Co_3O_4/CoO, BaO_2/BaO, Mn_2O_3/Mn_3O_4, CuO/Cu_2O), or nonstoichiometric redox compounds. Such compounds can be, for example, spinels expressed by the general formula AB_2O_4 or perovskites expressed by the general formula ABO_3, where A is a cation with a larger ionic radius and B is a relatively smaller cation [1,2,3]. Perovskites in particular, belong to the family of nonstoichiometric redox oxides compounds and are the main focus of the ABraytCSPfuture project. The generic redox oxide process scheme and the relevant ones for a stoichiometric (Co_3O_4) and a non-stoichiometric oxide (perovskite) material are shown below in Eq. (1a), Eq. (1b), and Eq. (1c), respectively.

$$MeO_x(s) + \Delta H \rightleftarrows MeO_{x-\delta}(s) + \delta/2\ O_2(g) \quad ...(1a)$$

$$Co_3O_4 + \Delta H \rightleftarrows 3CoO + 1/2\ O_2 \quad ...(1b)$$

$$ABO_3(s) + \Delta H \rightleftarrows ABO_{3-\delta}(s) + \delta/2\ O_2(g) \quad ...(1c)$$

Stoichiometric redox oxides are characterised by clearly defined specific weight change resulting from the non-continuous gain or loss of oxygen at a specific temperature that corresponds to a phase transition, that is why they are often also denoted as phase-change materials. Conversely, nonstoichiometric redox materials undergo partial reduction/oxidation without necessarily experiencing phase transition, exhibiting a continuous quasi-linear redox behaviour across a broad temperature range, which is

advantageous for coupling thermochemical and sensible heat storage. Additionally, these materials demonstrate improved performance in terms of thermal expansion under cyclic heating and cooling, as illustrated in Figure 1 [2].

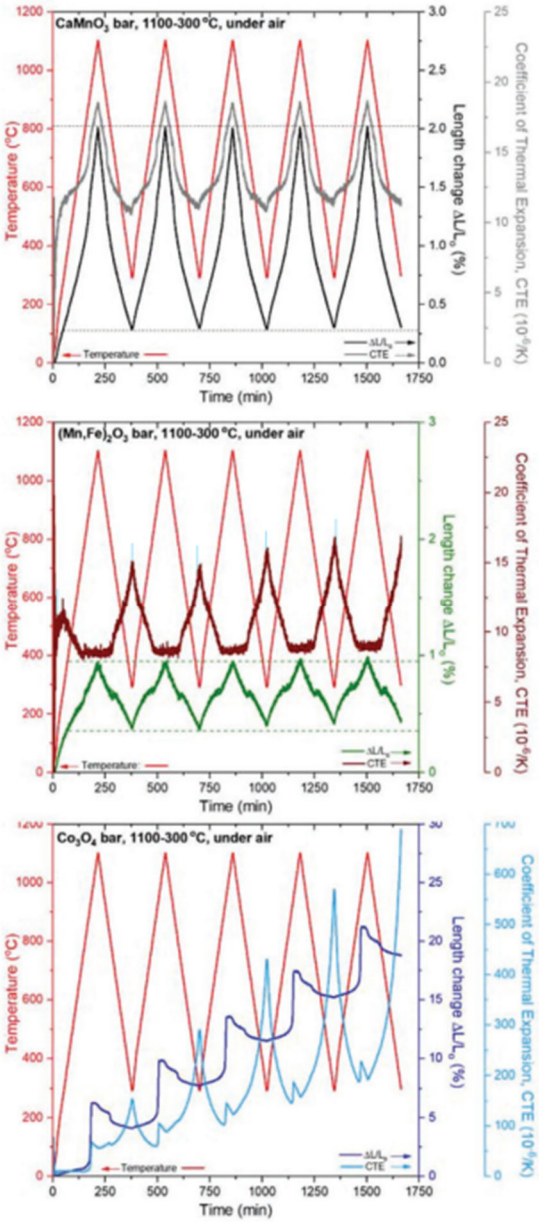

Figure 1: Cyclic thermal expansion of $CaMnO_3$ (top), $(Mn,Fe)_2O_3$ (middle), and Co_3O_4 (bottom) bar specimens. Measured by optical dilatometry in air and cycled between 300°C and 1100 °C [2].

As shown in Figure 1, the nonstoichiometric redox compound $CaMnO_3$ outperforms the stoichiometric redox oxides $(Mn,Fe)_2O_3$ and Co_3O_4, exhibiting a fully reversible thermal expansion of ≈ 2%, indicated in black, after cyclic heating and cooling, in contrast to $(Mn,Fe)_2O_3$ and Co_3O_4, which demonstrate irreversible thermal expansion. The length change curve ($\Delta l/l_0$) for $(Mn,Fe)_2O_3$, shown in green, is comparable to the one for $CaMnO_3$, with length change in the magnitude ≈ 1–2%, however, it presents a small, but clearly non-zero residual thermal expansion, which can also be observed in the CTE curve, depicted in burgundy color. Co_3O_4 displays a significant thermal expansion of as

high as ≈ 7% of its initial length after heating, with only a minor portion of this thermal expansion being recovered upon cooling, presenting a cumulative thermal expansion of ≈ 20% over just five cycles.

An essential parameter for sensible heat storage is heat capacity, a temperature-dependent property that indicates a material's ability to absorb thermal energy from its surroundings, mathematically expressed as the amount of energy required to raise the temperature by one unit, given by Eq. (2a), and when measured under constant pressure, the heat capacity expressed as Eq. (2b).

$$C = \frac{dQ}{dT} \quad \text{...(2a)}$$

$$C_P = \frac{dQ}{dT_P} \quad \text{...(2b)}$$

The heat capacity measurements for perovskite powders doped with Sr at the A-site are illustrated below, in Figure 2. Heat capacity measurements are crucial for materials selection, as higher heat capacity values (C_P) result in increased energy density through sensible heat to which the contribution of thermochemical energy storage (TCES) can be added, leading to more compact and effective storage systems. The experimental C_P values are within the range reported in the literature.

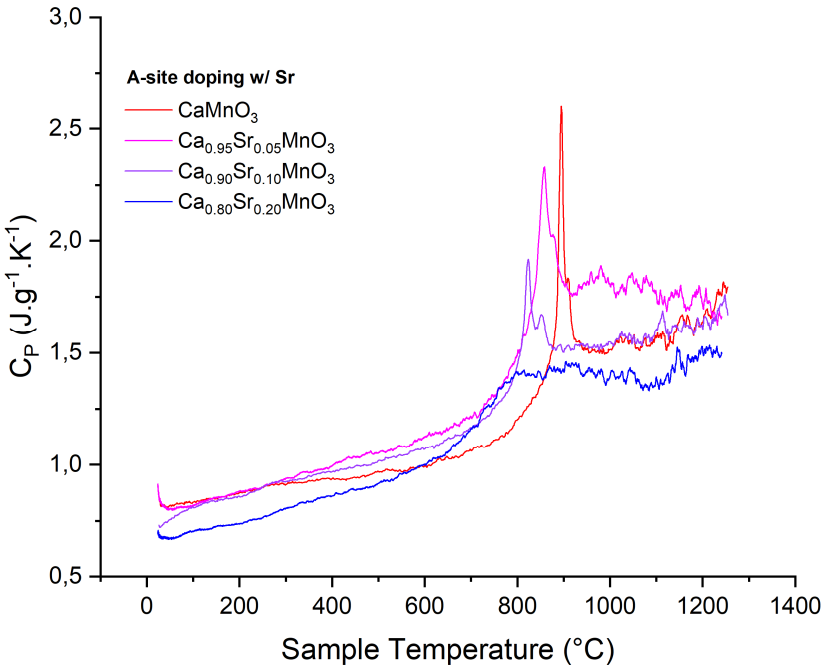

Figure 2: Specific Heat Capacity (C_P) Measurements for $CaMnO_3$ and A-site Sr-Doped $CaMnO_3$ Perovskites.

An evident trend in specific heat capacity (Cp) is observed, with Cp increasing as the temperature rises. In TCES systems, materials with high heat capacities are desirable because they are able to store more energy for a given temperature change, enhancing the system's overall efficiency. The peak in specific heat capacity (C_P) indicates a

significant energy input is needed to further increase the temperature, suggesting that the material can effectively store or absorb considerable amounts of thermal energy, as sensible heat. **However, this peak also indicates a phase transition that occurs within a narrow temperature range, leading to changes in the lattice parameters, which may intensify thermal stresses**. The intensity of the peak diminishes significantly with increasing concentrations of strontium as an A-site dopant. Ultimately, the peak vanishes at a strontium concentration of 20%, suggesting that the phase transition is inhibited by the dopant [4].

In Figure 3, cyclic thermal expansion measurements of $CaMnO_3$ perovskites with increasing strontium content as an A-site dopant are presented. All samples measured in air exhibited no residual thermal expansion. In the measurements conducted under a reducing atmosphere with 1% O_2, the samples with 5% and 10% strontium as an A-site dopant demonstrated the lowest residual thermal expansion, indicating potential superior performance.

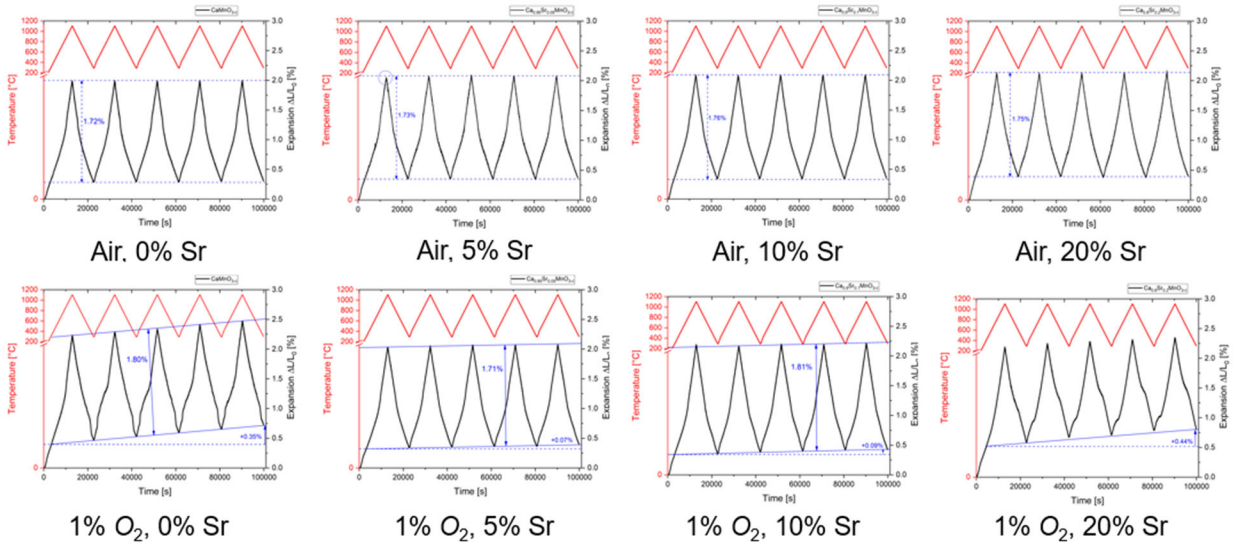

Figure 3: Cyclic thermal expansion of $Ca_{1-x}Mn_xO_3$ with increasing Sr content as an A-site dopant in air (top), and under a reducing atmosphere with 1% O_2 concentration (bottom) [4].

The objective of this project is to establish a system in which energy is transferred from a non-pressurised air stream to a pressurised air stream via using a ceramic redox material as the means to effectively connect these two and as heat storage medium at the same time, thereby enhancing the temperature of the latter to levels necessary for gas turbine air-Brayton cycles via dual-bed heat exchanger, functioning as a thermal booster made of redox oxide porous ceramics, which will operate by performing atmospheric pressure reduction and pressurised oxidation. Moreover, the proposed concept involves the use of porous structures arranged in cascades to optimise the efficiency of thermochemical application of redox materials within a given reactor volume, integrating diverse redox oxide materials, arranged in a deliberate spatial configuration tailored to their thermochemical properties and the temperature distribution of the heat transfer medium [1].

3. Thermomechanical behaviour of redox oxides applied to TCES

3.1 Thermal Stresses and Thermal Shock Resistance

When a solid body undergoes heating or cooling, its internal temperature distribution depends on its size, shape, thermal conductivity, and the rate of temperature change, which generates temperature gradients and results in differential dimensional changes that restrict the free expansion or contraction of adjacent volume elements. Consequently, thermal stresses arise in the material due to the temperature gradient across its dimensions and can be expressed as in Eq. (3).

$$\sigma_T = E\alpha_{Li}\Delta T_i \quad \ldots(3)$$

where E is the Young's Modulus, α_{Li} the linear coefficient of thermal expansion, and ΔT_i the temperature difference between two points in a direction i.

For ductile materials, thermal stresses can be alleviated through plastic deformation; however, the intrinsic non-ductile behaviour of most ceramics increases the risk of brittle fracture resulting from thermal stresses. Upon heating, the external surface of a specimen undergoes a more rapid temperature increase than its centre, resulting in greater expansion at the surface compared to the interior, generating compressive surface stresses directed towards its core. Conversely, thermal shock is more likely to occur during the cooling phase, as the induced surface stresses are of a tensile nature, which facilitates crack formation and propagation. Materials capable of withstanding severe thermal stresses without experiencing brittle fracture are referred to as thermal shock resistant. Thermal shock resistance depends on several thermal and mechanical properties of the material, such as Fracture Strength (σ_F), Thermal Conductivity (k), Young's Modulus (E), and Coefficient of Thermal Expansion (α_l, α_v). Ideally, to engineer a ceramic material with maximised Thermal Shock Resistance (TSR), it is desirable to attain high Fracture Strength (σ_F), high Thermal Conductivity (k), low Young's Modulus (E), and low Coefficient of Thermal Expansion (CTE: α_l, α_v) [5, 6]. The approximated expression for Thermal Shock Resistance is given below by Eq. (4).

$$TSR \cong \frac{k\sigma_F}{E\propto_L} \quad \ldots(4)$$

Ultimately, understanding the synergy among heat capacity, thermal conductivity, thermal expansion, and other material properties is crucial for designing ceramics that effectively manage thermal stresses and resist fractures in the context of thermochemical energy storage applications, thereby enhancing the efficiency and durability of energy storage systems, and leading to improved utilisation of thermal energy.

3.2 Thermal Conductivity

Heat transport in solids happens through two main mechanisms: lattice vibrations (k_l), also called phonons, and free electrons (k_e). The total thermal conductivity of a material is constituted by the sum of each mechanism contributions, given by $k = k_l + k_e$.

The thermal energy associated with phonons is transported in the direction of their motion, in which its heat transfer contribution results from the net movement of phonons from high to low temperature regions across a material exhibiting a temperature gradient.

The contribution of free electrons to thermal conductivity relies on the gain of kinetic energy in regions with higher temperature and the subsequent migration of these electrons to colder areas of the material. During this process, some of this energy is transferred to atoms through collisions with phonons or imperfections in the crystalline structure. Furthermore, the contribution of electronic thermal transport increases with the concentration of free electron.

In ceramics, the phonon mechanism is primarily responsible for the thermal conductivity, as ceramics, like other nonmetallic materials, are characterised by scarcity of free electrons. Consequently, the thermal conductivity is approximately equal to the lattice thermal conductivity, given by $k \approx k_l$, and ranging from 2 to 50 $Wm^{-1}K^{-1}$. The thermal conductivity of ceramics typically decreases with increasing temperature due to the scattering of lattice vibrations, which becomes more pronounced at elevated temperatures.

Porosity is another significant factor that dramatically influences thermal conductivity, as an increase in the pore volume — typically filled with air, which has a very low thermal conductivity of $k_{air} = 0.02$ $Wm^{-1}K^{-1}$ — results in a decrease in thermal conductivity [5, 6].

3.3 Thermal Expansion

The majority of solid materials expands upon heating and contracts when under cooling. Thermal expansion is a property that quantifies the extent to which a material expands upon heating, and it can be mathematically described, when considering a unidimensional thermal expansion, as in Eq. (5a).

$$\frac{\Delta l}{l_0} = \alpha_L \Delta T \quad \text{...(5a)}$$

Where Δl is the variation in length experienced by the specimen, l_0 is the initial length, ΔT is the temperature change and α_L is the linear coefficient of thermal expansion. If considering the volumetric thermal expansion, the expression is given by Eq. (5b).

$$\frac{\Delta v}{v_0} = \alpha_V \Delta T \quad \text{...(5b)}$$

From the atomic perspective, the macroscopic thermal expansion is resulted by an increase in the average interatomic distances during heating.

Due to their relatively strong interatomic bonding forces, many ceramic materials exhibit comparatively low coefficients of thermal expansion, typically ranging from approximately 5E-7 to 1.5E-5 K^{-1}. Ceramic materials subjected to significant cyclic temperature changes must present low coefficients of thermal expansion and display isotropy. All non-crystalline ceramics and ceramics with cubic crystalline structures are isotropic. Failure to meet these criteria may result in fracture due to nonuniform dimensional changes, a phenomenon known as thermal shock. If these criteria are not met, the materials may be prone to fracture due to nonuniform dimensional changes, a phenomenon referred to as thermal shock [5].

4. Finite Element Method (FEM)

The laws of physics related to space- and time-dependent problems are generally expressed in terms of Partial Differential Equations (PDEs). For the majority of geometries and problems, analytical solutions to these PDEs are often unattainable. Consequently, approximations of the equations are typically developed, relying on various discretisation techniques, which allow for the approximation of the PDEs by numerical model equations, that can then be solved using numerical methods. The solutions obtained from these numerical model equations represent approximations of the true solutions to the PDEs. The Finite Element Method (FEM) is commonly utilised for computing such approximations. FEM is extensively applied in solid mechanics, fluid mechanics, and thermodynamics, grounded in the principle of variation and incorporating concepts from finite difference schemes and block polynomial interpolation. The efficiency and accuracy of the solution depends on data such as material properties, geometry, and boundary conditions [7, 8].

In solid mechanics, the finite element method (FEM) is employed to determine the deformation or displacement of a structure under external loads. When evaluating thermomechanical behaviour, temperature gradients can be either partially or completely responsible for the internal stress state by generating fields of thermal stresses. Given the complexity of solving these displacements analytically, approximate numerical methods are typically used. FEM involves dividing a continuous object into smaller regions called finite elements. By applying governing equations and using polynomial interpolation through a variation method, the displacement in each element is calculated [7].

The process of dividing an object into many small elements is called discretisation. Meshing an object consists of partitioning it into smaller elements, where the connections between these elements are referred to as nodes. Figure 4 presents the graphical representation of the optical dilatometry specimen (shown in Figure 5 below) created in *OpenFOAM*, utilizing the open-source visualisation application *ParaView*®.

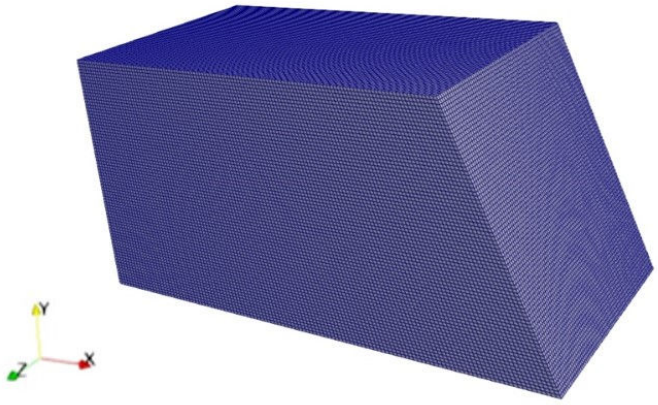

Figure 4: Graphical representation of the optical dilatometry specimen created in *OpenFOAM*, utilizing the open-source visualisation application *ParaView®*

Although there are no strict constraints on element size, effective meshing must strike a balance between the computational resources and the necessary computational accuracy. Key considerations include:

1) Guaranteeing that the vertex of an element is also a vertex of a neighbouring element;

2) Avoiding large obtuse angles and high edge ratios;

3) Ensuring grid refinement in areas with steep gradients, and the use of coarser grids in regions with smoother gradients;

4) Minimising the maximum difference between node numbers of adjacent nodes to reduce the stiffness matrix bandwidth and computing load.

Over decades of development in the finite element method, various element types have been created. To choose the most suitable element type, one must consider the process to which the object is subjected and the object's structural shape. For a 1D object, a two-node line element is suitable; for a 2D object, either a three-node triangle element or a four-node quadrangle element can be used; and for a 3D object, an eight-node hexahedron element is appropriate.

It is generally assumed that the dependent variables, such as displacement, vary linearly within each element, which results in a representation using discrete linear functions, referred to as shape functions, that describe the distribution of these variables. By incorporating a finite number of parameters, the equation is transformed into an algebraic expression with finite degrees of freedom, which is essentially a polynomial interpolation function, as given in Eq. (6).

$$u = N_1 u_1 + N_2 u_2 + \cdots + N_m u_m \quad \ldots(6)$$

Considering the solid mechanics problem, u_k (k = 1, 2, ..., m) represent the displacements at the nodes of this element, N_k (k = 1, 2, ..., m), thus, the function displacement is described as in Eq. (7).

$$u(x) = \frac{x_{i+1}-x}{x_{i+1}-x_i} u_i \frac{+x-x_i}{x_{i+1}-x_i} u_{i+1},\ x_i \leq x \leq x_{i+1} \quad \ldots(7)$$

The effectiveness of a material model in Finite Element Analysis depends on the selection of appropriate constitutive equations. Such equations are generally established through mechanical experiments and constitutive theories. For numerical computations related to significant deformations, material models must comply with relevant constitutive theories, ensuring they are independent of coordinate systems and accurately depict both the nonlinear geometry of large deformations and the nonlinear physical relationships of the materials. The governing equations of the finite element method are derived from the variation principle, utilizing two common approaches: the energy method and the weighted residual method [7]. The following considerations outlines several fundamental aspects of the formulation of the finite element method.

i. Independence of Variables: The solution for field variables initially does not depend on either the differential equation or boundary conditions, leading to an assumed trial solution that satisfies boundary conditions.
ii. Residuals: The trial solution typically does not satisfy the differential equation, resulting in an error known as the residual.
iii. Residual Management: Residuals cannot generally be reduced to zero throughout the entire domain, but can be minimised at selected points. A common approach is to make the weighted sum of the residuals equal to zero over the entire domain.
iv. Improving Accuracy: The accuracy of the trial solution can be enhanced by incorporating higher-order terms; however, this increases computational complexity and the associated resource requirements.
v. Domain Discretization: The domain is discretised into a finite number of elements, with piecewise trial functions assigned to each segment.
vi. Shape Functions: The trial functions for each element are referred to as shape functions, which use interpolation to estimate field variable values within the element, with endpoints referred to as nodes.
vii. Weighted Sums: Using the shape functions, a weighted sum is computed for each element and then aggregated for the entire domain.
viii. Global Characteristic Matrix: Consistent shape functions across elements lead to identical computations, resulting in element characteristic matrices, which are summed to form the global characteristic matrix, or global stiffness matrix.

To summarise, FEM entails partitioning the entire problem domain into a finite number of subdomains referred to as elements. Initially, a property matrix is computed for each element, which is subsequently assembled to construct a global matrix representing the entire domain. By incorporating the global matrix with the associated force vector, an algebraic equation is formulated in accordance with the specified boundary conditions. This system of equations, which may feature eigenvalue problems, is then solved to determine the unknown field variables [8].

5. 1st version of thermomechanical simulation

In this section, a glance at the first version of the simulation methodology and preliminary results for the thermochemical expansion of redox structures are presented. It aims to integrate thermomechanical simulations and stress analysis to assess the combined contributions of thermal and chemical reactions to the dimensional changes of ceramic objects, as well as the critical stresses arising from oxide compositions. The input data is based on key characteristics of the porous objects derived from literature data or obtained through experimental measurements.

The first version of the thermal simulation focuses on recreating the measurement of the linear coefficient of thermal expansion for $CaMnO_3$, as reported in [2]. In that study, dilatometry experiments were conducted using parallelepiped-shaped specimens with dimensions of 10-8 x 5 x 5 mm in a contactless optical dilatometer (L74/HS/1600, Linseis, Selb, Germany). These specimens were sectioned from larger bars with a total porosity of 10.8%, produced by uniaxial cold compression of single-phase, ground $CaMnO_3$ powder, followed by sintering at 1350 °C for 20 hours, as described in Table 1.

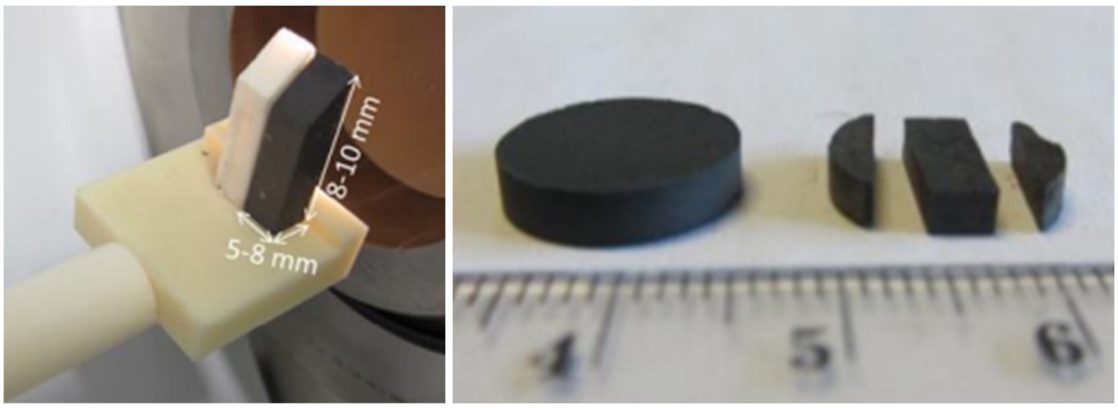

Figure 5a and b: Dilatometry experiments specimens.
a. Left: $CaMnO_3$; and **b.** Right. Co_3O_4 and $(Mn,Fe)_2O_3$ [2].

Comparative dilatometry tests were conducted on two additional redox oxide systems, Co_3O_4 and $(Mn,Fe)_2O_3$, as discussed in Section *2. Redox Oxides Applied to TCES*. These systems were previously analysed in a TGA/DSC setup for weight changes and thermal effects in conjunction with various perovskite compositions, including $CaMnO_3$. Specimens were cut from pellets sintered at 1000 °C and 1450 °C for Co_3O_4 and $(Mn,Fe)_2O_3$, respectively, as reported in Table 1. The dilatometry specimens for Co_3O_4 and $(Mn,Fe)_2O_3$ are shown in Figure 5b.

Table 1: Thermal history of specimens used for dilatometry experiments reported in [2].

Composition	Specimen	Sintering Temperature (°C)	Sintering Time (h)
$CaMnO_3$	Bar	1350	20
Co_3O_4	Pellet	1000	4
$(Mn,Fe)_2O_3$	Pellet	1450	4

All dilatometry experiments were carried out in air, following a consistent 5-cycle heating and cooling protocol for comparability [2]. The cyclic heating and cooling protocol for the dilatometry experiment was structured as follows: the specimen was initially heated from room temperature to 1100 °C, then cooled to 300 °C. This was followed by repeated cycles of heating from 300 °C to 1100 °C and cooling from 1100 °C to 300 °C, with a heating rate of 5 °C/min and a cooling rate of -5 °C/min respectively.

The protocols and setup features from the dilatometer experiments were translated into boundary conditions, as illustrated in Figure 6, which represents the temperature boundary conditions for each face of the ceramic body. The source of thermal energy is radiative heat flux, which is calculated by considering the specimen's dimensions and properties, such as specific heat (c), relative density (ρ_R), porosity ($\%_{Porosity}$), and the relevant temperature range (ΔT) for the heat transport problem.

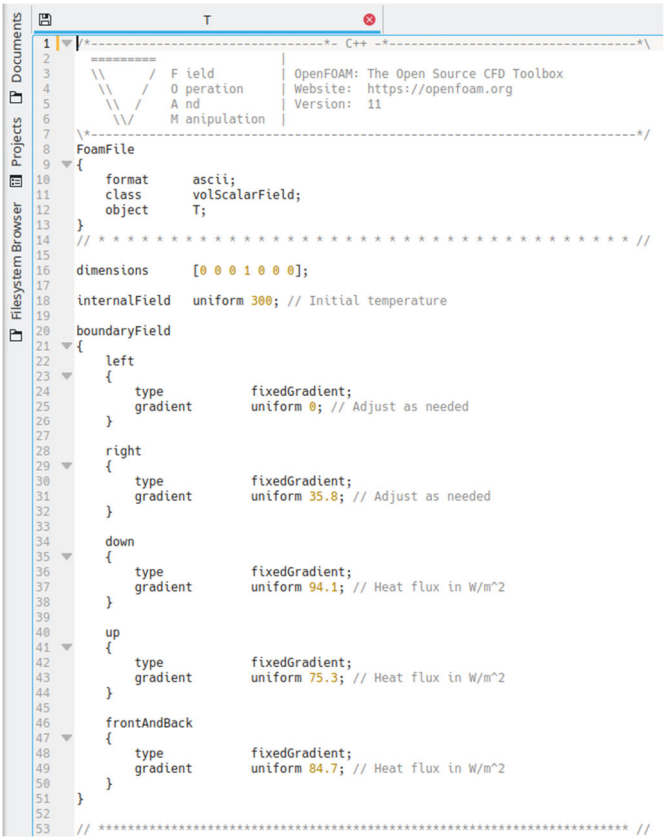

Figure 6: *OpenFOAM* boundary condition dictionary *T* (Temperature), where the heat source is defined as a calculated radiative heat flux.

The software employed in this initial simulation version was *OpenFoam® v11*. *OpenFOAM®*, which stands for *Open Field Operation And Manipulation*, is a C++ framework tailored for the creation of customised numerical solvers and pre-/post-processing tools that address continuum mechanics issues, particularly in the realm of *Computational Fluid Dynamics* (CFD). However, this choice is not definitive, as alternative software options, including *ANSYS®* and *COMSOL®*, are currently under consideration for the continued simulation work [9, 10, 11]. A comparative analysis of the advantages and disadvantages of these software options will be provided in Section 6.

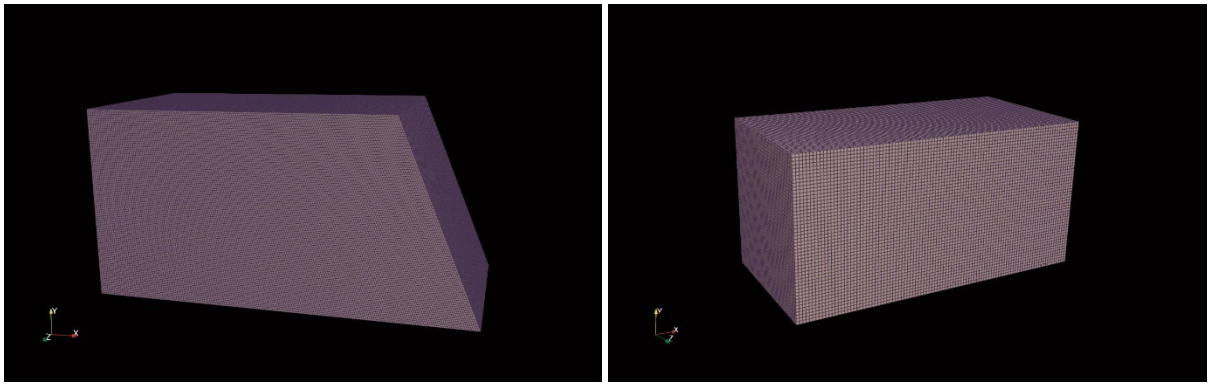

Figures 7a and 7b: Representation of specimens for dilatometry experiments in *OpenFOAM® v11*. **a.** Left: Optical dilatometry; and **b.** Right: Push-rod dilatometry.

OpenFOAM® v11 is implemented in *C++* and features a code structure that includes .C files, which contain the actual implementation, and .H files, which provide interfaces that enable access to functions, global variables, and macros from other files. Initial and boundary conditions, along with material properties, geometries, and meshing features, are specified as inputs in dictionaries [9]. Figure 7a and 7b present the geometry and meshing implementation in *OpenFOAM®*, which models the types of dilatometry specimens utilised in experiments. Furthermore, the framework supports the use of modified pre-existing solvers to address specific simulation requirements.

A widely adopted approach for conducting thermomechanical simulations to analyse the stress state and dimensional changes of a ceramic body—such as $CaMnO_3$ perovskite—subjected to cyclic heating and cooling involves partitioning the problem into two principal components: heat transfer simulation and solid mechanics simulation, illustrated in Figures 8a, 8b and 8c.

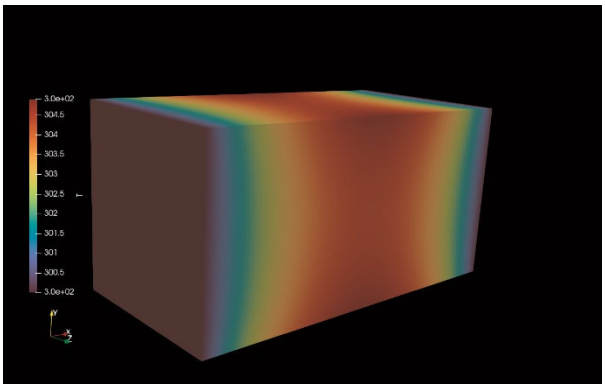

Figures 8a: Visualisation of Heat Transfer Simulation in *OpenFOAM v11* via *ParaView*.
a. Centre: Temperature (T).

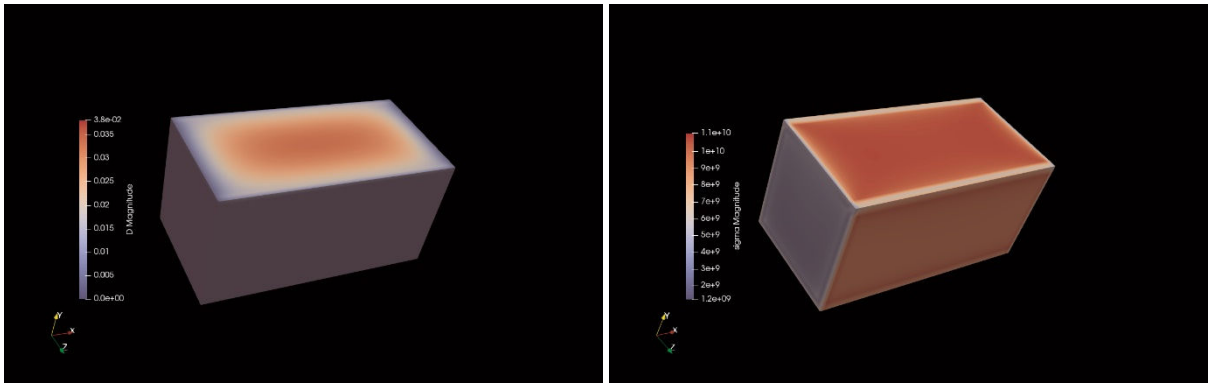

Figures 8b and 8c: Visualisation of Solid Mechanics Simulations in *OpenFOAM v11* via *ParaView*.
b. Left: Displacement (D); and **c.** Right: Stress (Sigma, σ).

First, the heat transfer equations are solved using an appropriate model, which includes selecting the relevant partial differential equations, boundary conditions, and material properties. Table 2 presents the properties incorporated as inputs in *OpenFOAM®*. The resultant thermal profiles at various time increments are then integrated into the coupled solid mechanics framework. This coupling facilitates the generation of chronological stress state profiles and corresponding displacements, effectively modelling the thermochemical expansion during heating, and contraction during cooling.

Throughout the development of this simulation, the reference perovskite composition of $CaMnO_3$ has been the sole subject of interest. Consequently, its physical, chemical, mechanical, thermal, and thermomechanical properties have been assessed for incorporation into this simulation. The initial aim of this model is to simulate conditions for a ceramic body that replicates the properties, dimensions, and shape of the dilatometry specimens, applicable to both the conventional push-rod test and cyclic measurements using an optical dilatometer. This model will subsequently contribute to the primary objective of this deliverable: a comprehensive study on thermal expansion, thermal stresses, and thermal shock resistance, particularly concerning variations in microstructural characteristics such as porosity and microcracking state.

Inspired by a study on cordierite honeycomb structures that focussed on the temperature dependence of the effective Young's modulus, coefficient of thermal expansion, and other properties in porous polycrystalline ceramics [12], the present investigation aims to conduct a detailed analysis of thermal stresses. Specifically, the referred study on cordierites targeted the examination of microstresses generated during cyclic heating and cooling, as microcracking primarily arise during the cooling phase [5, 6]. Microstresses arise from the mismatch in thermal expansion and elastic properties among anisotropic, randomly oriented grains [5, 6, 12]. Moreover, this study aimed to explore how variations in porosity influenced the mechanical and thermomechanical properties of cordierites. This research intends to evaluate the potential for drawing parallels between the findings of the referenced study on cordierites and the relevant perovskites compositions. Additionally, it aims to investigate the applicability of the microcracking mitigation mechanisms identified in cordierites at specific temperature drops to perovskites, as indirectly indicated by thermal expansion data [12].

Table 2: Relevant Properties for Heat Transfer and Solid Mechanics Simulations.

Properties/Inputs for Thermal Stresses Simulations

OpenFOAM® v11

Symbol	Unit	Property
m	[kg]	*Mass*
V	[m^3]	*Volume*
L_0	[m]	*Dilatometry specimen initial length*
ΔL	[m]	*Thermal Expansion*
α_L	[K^{-1}]	*Linear Coefficient of Thermal Expansion*
α_V	[K^{-1}]	*Volumetric Coefficient of Thermal Expansion*
T_0	[K]	*Initial Temperature*
T_F	[K]	*Final Temperature*
P_0	[Pa]	*Initial Pressure*
P_F	[Pa]	*Final Pressure*
k	[$Wm^{-1}K^{-1}$]	*Thermal Condutivity*
ρ	[kgm^{-3}]	*Density*
ν	[dimless]	*Poisson's Ratio*
G_v	[Pa]	*Shear Stress*
E	[Pa]	*Young's Modulus*
C_p	[$Jkg^{-1}K^{-1}$]	*Specific Heat Capacity (const. Pressure)*
(Coeffs)C_p	[$Jkg^{-1}K^{-1}$]	*Specific Heat Capacity Polynomial Coefficients (const. Pressure)*
C_V	[$Jkg^{-1}K^{-1}$]	*Specific Heat Capacity (const. Volume)*
(Coeffs)C_V	[$Jkg^{-1}K^{-1}$]	*Specific Heat Capacity Polynomial Coefficients (const. Volume)*
H_F	[Jkg^{-1}]	*Formation Enthalpy*
S_F	[$Jkg^{-1}K^{-1}$]	*Formation/Standard Entropy*

6. Software selection for thermal stress analysis: comparative analysis of ANSYS®, COMSOL®, and OpenFOAM®

In the field of thermomechanical simulations, selecting the appropriate software is crucial for achieving reliable results composition. This table provides a comparative overview of three prominent software packages: *ANSYS*®, *COMSOL*®, and *OpenFOAM*®. Each software offers unique capabilities and features tailored to different aspects of thermomechanical analysis. *ANSYS*® is well-regarded for its robust finite element analysis (FEA) tools, making it suitable for complex structural simulations. *COMSOL*®, with its multiphysics approach, excels in integrating various physical phenomena, allowing for detailed analysis of coupled thermal and mechanical interactions. *OpenFOAM*®, an open-source option, provides extensive customization and flexibility, particularly for fluid dynamics and thermodynamic simulations. Table 3 presents a comparison that highlights the key features, strengths, and limitations of each software, serving as an aid for making informed decisions based on specific simulation needs.

Table 3: Cross-Comparison of ANSYS, COMSOL, and OpenFOAM in Thermomechanical Analysis

Feature/Criteria	OpenFOAM	ANSYS	COMSOL
Type of Software	Open-source CFD toolbox	Commercial software suite	Commercial multiphysics software
Thermomechanical Analysis	Basic solid mechanics features	Yes	Yes
Cyclic Heating/Cooling	Supports transient heat transfer; custom solvers can be developed	Comprehensive support with built-in modules	Robust support with time-dependent studies
Porosity Assessment	Can model porous media; requires custom definitions	Porous media module available; easy integration	Built-in porous media features; user-friendly interface
User Interface	Command-line based; limited GUI	Comprehensive GUI; user-friendly	Intuitive GUI; graphical modelling
Documentation & Support	Extensive community support; varied documentation	Professional support; extensive documentation	Professional support; extensive and detailed documentation
Customization	Highly customizable; requires programming knowledge	Custom scripts possible; extensive user control	Customisation via COMSOL script language
Multi-physics Capabilities	Focusses mostly in CFD, therefore, it presents strong features for integration of mass and heat transport.	Strong multi-physics capabilities	Excellent multi-physics capabilities with easy coupling
Solver Options	Various solvers available; customizable	Advanced solvers; easy to switch	Robust solvers; can use built-in solvers
Post-processing	Basic visualization tools; integration with external tools (e.g., ParaView)	Advanced post-processing tools; built-in capabilities	Comprehensive post-processing features; visualisation tools
Cost	Free (open-source)	Commercial licensing costs	Commercial licensing costs

OpenFOAM® has exhibited strong performance in addressing heat transfer problems; however, its standard ***solid mechanics*** package is insufficient for conducting reliable thermomechanical analyses, as it does not support fatigue analysis and lacks the capability to assess whether the stresses induced by specific boundary conditions exceed critical stress levels. Furthermore, in addition to the limitations of its basic solid mechanics capabilities and the steep learning curve associated with its less user-friendly interface, the computational resources required to perform thermomechanical simulations in *OpenFOAM*® are considerably high [9]. *ANSYS*® provides robust tools for conducting detailed fatigue analysis, enabling the assessment of thermomechanical material behaviour under cyclic loading conditions. However, its limited customisation options may restrict flexibility for specialised applications, and it can experience performance issues when handling very large or complex models, often necessitating high-performance computing resources [10]. *COMSOL*® offers particularly strong multiphysics capabilities, which facilitate seamless coupling of thermal and mechanical processes. Its user-friendly interface facilitates straightforward setup and visualisation of simulations, while the Application Builder offers customization and flexibility for tailored applications. Additionally, *COMSOL*® features integrated post-processing tools for thorough analysis of results [11]. However, it can be costly, particularly for users requiring multiple modules, and may encounter performance issues when simulating large or complex models. Its solid mechanics features may also be less extensive than those found in dedicated structural analysis software like *ANSYS*®. To undertake a thermomechanical analysis of redox oxide porous structures utilized in thermochemical energy storage with *COMSOL*®, it is imperative to incorporate the modules for heat transfer, structural mechanics, and porous media flow.

Microstructure modeling and visualisation capabilities in *ANSYS*®, *COMSOL*®, and *OpenFOAM*® vary significantly in thermomechanical analysis. *ANSYS*® offers advanced tools for incorporating detailed microstructural properties and effective post-processing visualisation of their effects on thermomechanical behavior. *COMSOL*® supports microstructure modeling through its multiphysics environment, enabling integration into broader analyses and providing insightful visualisation tools. In contrast, *OpenFOAM*®, while primarily focussed on computer fluid dynamics, allows for customizable microstructure modeling through coding and external visualisation tools like *ParaView*®, requiring more effort for implementation. Overall, *ANSYS*® and *COMSOL*® provide more user-friendly and integrated solutions, while *OpenFOAM*® offers flexibility at the expense of complexity.

All three software options—*ANSYS*®, *COMSOL*®, and *OpenFOAM*®—can utilise ***computed tomography scan*** (CT Scan) data that can be obtained in the partners' facilities – a typical one of a $CaMnO_3$ foam is shown in Figure 9 - to create geometries, though their capabilities but their processes differ. *ANSYS*® offers tools for importing and processing CT Scan data, enabling the creation of detailed geometries through its SpaceClaim module. *COMSOL*® supports importing image data, including CT Scans, via its Image Processing Module, allowing users to convert scanned data into usable geometries for simulations. In contrast, *OpenFOAM*® does not have built-in tools for directly importing CT Scan data;

users must rather pre-process the data using external software to convert it into compatible formats before importing. In summary, *ANSYS*® and *COMSOL*® provide more integrated solutions, while *OpenFOAM*® requires additional steps for data preparation, at the expense of being an open-source software.

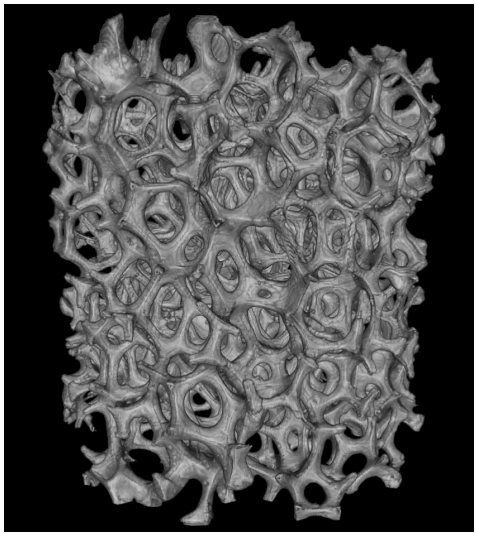

Figure9: Computed tomography scan image of a $CaMnO_3$ foam obtained by DLR.

Post-processing capabilities vary among *ANSYS*®, *COMSOL*®, and *OpenFOAM*®. *ANSYS*® features a comprehensive post-processing module that allows for detailed visualisation and analysis of results, making it user-friendly for interpreting complex data. *COMSOL*® also offers robust post-processing tools with an emphasis on multiphysics visualisation, allowing users to easily manipulate and display results from various coupled simulations. In contrast, *OpenFOAM*® requires more manual intervention for post-processing, often involving command-line tools or external software like *ParaView*®, which may present a steeper learning curve but allows for greater customization and flexibility in data visualisation. Therefore, a decision on which software should be employed as the solid mechanics application to be coupled with the heat transfer simulation results has not yet been reached.

Taking all these factors into account, a decision regarding which software should be utilized as the solid mechanics application to be coupled with the heat transfer simulation results has yet to be determined.

7. Next steps and Density Functional Theory (DFT) calculations

The forthcoming steps are as follows:

1) Select an appropriate solid mechanics application to couple with the *OpenFOAM*® heat transfer simulation.
2) Transfer the developed work to the Terrabyte Data Analytics joint platform, a collaboration between DLR and LRZ, to reduce computational processing times.

3) Incorporate pores into the graphical representation, which has so far been described as a uniform object, in order to enhance the overall porosity of the ceramic body.

The FEM simulation is intended to be integrated with DFT calculations of material properties, illustrated in Figure 10. DFT calculations provide a comprehensive framework for understanding and predicting the properties of materials by leveraging the fundamental relationship between electron density and material behaviour.

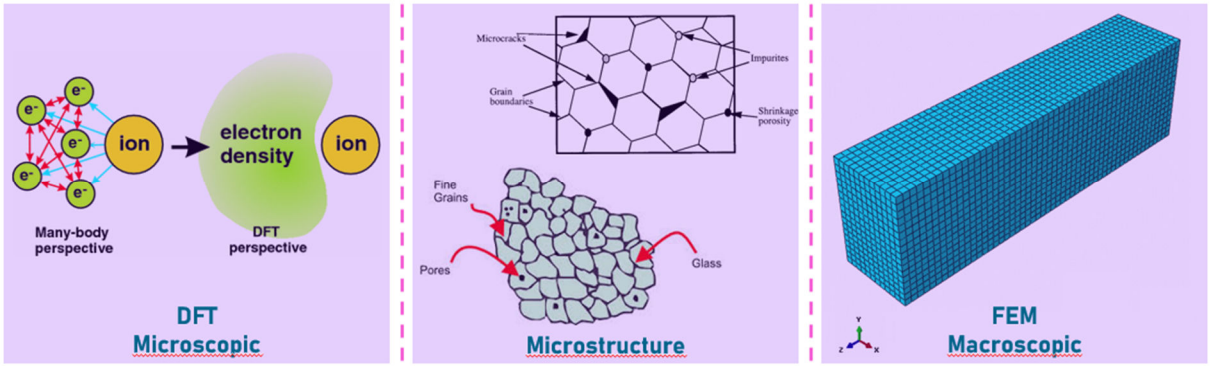

Figure 10: Illustration of DFT principles (left), applied here to material property calculations for FEM analysis (right). However, the influence of microstructure (centre) remains unclear, as DFT is unable to account for its effects.

In fact, apart from reaction thermochemistry, the computational materials screening in Task 2.1 also included the comparison of materials based on their mechanical properties, sensible heat storage capabilities, and volume expansion upon reduction or oxidation. Understanding how composition affects the thermal and mechanical properties of perovskite oxide ceramics is crucial to rationally guide a materials optimization towards porous bodies with improved cycling stabilities and lifetime. In Task 4.2 such an optimization is foreseen to be performed based on the multi-physics modelling of porous ceramic bodies, but strategies to modify the underlying materials properties are necessary to steer this process in the desired direction. In WP2, specifically $CaMnO_3$-based compositions were identified as some of the most promising ones for thermochemical energy storage. Using an existing regression analysis model [13], the elastic constants of these compounds and their heat capacities were calculated for $Sr_xCa_{1-x}MnO_3$ compositions with x = 0.0 … 0.5 based on theoretical results reported in a high-throughput DFT database [14]. The obtained Young's moduli and average gravimetric heat capacities in the temperature range 300 - 1100°C are shown in Figure 11. With increasing Sr content, the Young's modulus of the material drops which is generally associated with a lower theoretical tensile strength in ceramic materials. A possible explanation for this behaviour is the reported lower bond strength of Sr-O compared to Ca-O bonds which results in, for example, smaller elastic constants for SrO compared to CaO [15]. This finding suggests that dopants with stronger bonds to O could enhance the material's resilience towards elastic deformation and potentially crack formation. While the sensible heat stored per mole of material only slightly varies between different $Sr_xCa_{1-x}MnO_3$ compounds as shown in Figure 2 (less than 0.5% change between x = 0.0 and x = 0.5), the gravimetric sensible heat storage capability drops significantly in the temperature range 300 - 1100°C upon doping. This drop is caused by the larger atomic mass of Sr compared to Ca. Furthermore, due to the increasing molar volume of $Sr_xCa_{1-x}MnO_3$ with increasing Sr content (due to the longer Sr-O bonds) the volumetric sensible energy density is reduced as well. However, this drop in sensible energy density is offset by an increased chemical heat

component. Based on DFT calculations performed at DLR, the chemical heat storage component of $CaMnO_3$ is expected to significantly increase with Sr dopants concentrations around ~10% (relative to Ca) due to the lower reduction enthalpy of doped $Sr_xCa_{1-x}MnO_{3-\delta}$ as shown in 4.5.b. In our extended *in silico* screening, an upper limit of ~380 kJ/mol O_2 was assumed based on the molar entropy of O_2 and typical error ranges of DFT redox enthalpies reported in literature. The reduction plateaus in the approximate δ-ΔH curves in 4.5.b suggest a significantly larger reduction extent below this upper enthalpy limit for an 80-atom $CaMnO_3$ simulation cell with two Sr dopants (corresponding to x = 0.125) compared to a pristine one with final δ values of 0.25 and 0.125, respectively, which is in good agreement with previous experimental literature reports [4].

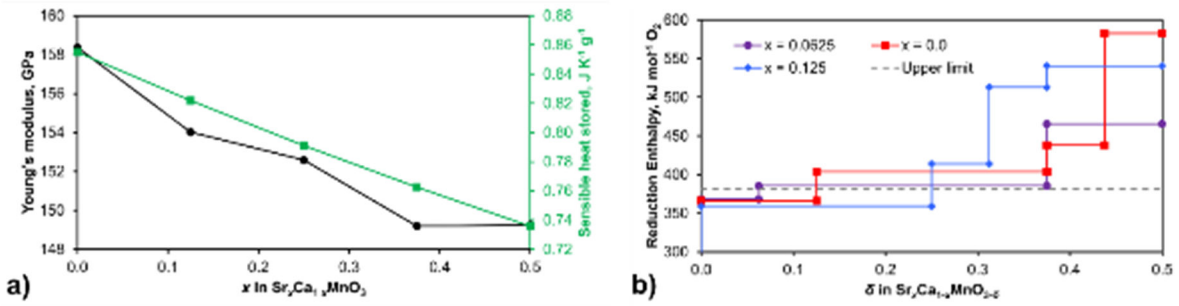

Figure 11. (a) Theoretical Young's moduli and sensible energy density of Sr-doped $CaMnO_3$ with increasing Sr content. (b) First-principles reduction enthalpies of pristine and Sr-doped $CaMnO_3$ depending on the degree of reduction δ. The dashed line indicates the position of the theoretical upper enthalpy limit.

Based on the computed lattice parameter changes for stable reduced phases below the upper enthalpy limit, average chemical volume expansions can be computed. An example for orthorhombic $CaMnO_3$ and $Sr_{0.125}Ca_{0.875}MnO_3$ with a typical δ value of 0.1 is presented in Table 4. The computed increase of chemical expansion with Sr doping is in qualitative agreement with previous experimental results [4]. $CaMnO_3$ is further known to undergo a transition between an orthorhombic and a cubic phase above ~800°C (Figure2). As shown in Table 4.1 the volume change during this phase transition results in a significantly lower volume expansion in the presence of Sr doping due to a reduced orthorhombic distortion in the doped compound as was suggested before [4].

Table 4: Computed chemical volume and phase transition expansion for pristine and Sr-doped $CaMnO_3$.

Composition	Chemical volume expansion for δ = 0.1 in %	Orthorhombic-cubic phase transition expansion in %
$CaMnO_3$	0.96	0.82
$Sr_{0.125}Ca_{0.875}MnO_3$	1.18	<0.01

These preliminary first-principles simulation results indicate on one hand potential strategies to tune thermo-mechanical materials properties like elastic constants or specific/volumetric heat capacities via doping. On the other hand, they can provide estimated values for materials properties which are not easily assessible from experiments (like the isolated chemical heat or volume expansion) for various Sr-doped $CaMnO_3$ compositions to supplement the planned numerical modelling of thermo-mechanical stresses in porous perovskite structures.

8. Summary

Literature indicates that $CaMnO_3$-based compositions have the potential for application in thermochemical energy storage (TCES) due to their lack of or substantially low residual thermal expansion, exhibiting only or mostly non-residual thermal expansion during cyclic heating and cooling [2, 4]. Consequently, it is essential to investigate the thermal stresses generated within the ceramic body as a result of induced temperature gradients during these processes. Understanding critical stress levels and the distribution of dimensional expansion is crucial for designing components and systems capable of withstanding thermal shock.

The present investigation focusses on the influence of varying porosity levels on the mechanical and thermomechanical behaviour of perovskites under cyclic thermal stresses conditions. An initial simulation of thermal stresses is currently under development, aimed at evaluating the thermal expansion and stress distribution within a compacted ceramic body made from $CaMnO_3$ powder with 10.8% porosity.

The thermomechanical evaluation is being conducted in two steps: the calculation of thermal profiles through a heat transfer simulation, followed by their integration into a solid mechanics application to evaluate the generated stresses. The heat transfer simulation produces thermal profiles that will be input into the solid mechanics application, enabling the calculation of thermal expansion and stress levels, as well as their distribution, for comparison with experimental critical stress values and existing literature. However, several challenges have arisen, including extended computational times and the selection of the most suitable solid mechanics applications to couple with the *OpenFOAM*® heat transfer simulation.

The FEM simulation is intended to be integrated with DFT calculations of material properties, that provide a comprehensive framework for understanding and predicting the properties of materials by leveraging the fundamental relationship between electron density and material behaviour.

9. References

[1] C. Agrafiotis, M. Roeb, C. Sattler. *Exploitation of thermochemical cycles based on solid oxide redox systems for thermochemical storage of solar heat. Part 4: Screening of oxides for use in cascaded thermochemical storage concepts*, Solar Energy, 139, 695-710 (2016).

[2] M. Pein, L. Matzel, L. de Oliveira, G. Alkan, A. Francke, P. Mechnich, C. Agrafiotis, M. Roeb, C. Sattler. *Reticulated Porous Perovskite Structures for Thermochemical Solar Energy*, Advanced Energy Materials, 12, 695-710 (2022). https://doi.org/10.1002/aenm.202102882.

[3] V.M. Goldschmidt. *Die Gesetze der Krystallochemie*. Naturwissenschaften, 14 (21), 477-485 (1926).

[4] L. Klaas, M. Pein, P. Mechnich, A. Francke, D. Giasafaki, D. Kriechbaumer, C. Agrafiotis, M. Roeb, C. Sattler. Controlling thermal expansion and phase transitions in $Ca_{1-x}Sr_xMnO_3$ by Sr-content. Phys. Chem. Chem. Phys., 24, 27976 (2022).
[5] W. D. Callister Jr., D. G. Rethwisch. Materials Science and Engineering. Chapter 12 - Structures and Properties of Ceramics (p.458-463), Chapter 19 - Thermal Properties p.742-753. Willey, Global Edition, ISBN 978-1-11-945391-8 (2020).
[6] J. F. Shackelford Jr. Introduction to Materials Science for Engineers. Chapter 6 - Mechanical Behaviour (p.164-167), Chapter 7 - Thermal Behaviour (p.210-223). Pearson, 8th Edition, ISBN 978-0-13-382665-4 (2014).

[7] S. Nayak, S. Chakraverty. Interval Finite Element Method with MATLAB. Chapter 2 - Interval Finite Element Method (p.7-17), Academic Press, ISBN 9780128129739 (2018).

[8] L. Wang. Foundations of Stress Waves. Chapter 12 - Numerical Methods for Stress Wave Propagation (p.475-509), Elsevier Science, ISBN 978-0-08-044494-9 (2007).

[9] H. G. Weller, G. Tabor, H. Jasak, C. Fureby. A tensorial approach to computational continuum mechanics using object-oriented techniques. Computers in Physics, Vol. 12, N. 6 (1998).

[10] ANSYS® Mechanical Application 2024 R2, System Coupling C++ library 2024 R2 Documentation (2024).

[11] COMSOL® Multiphysics 4.3b, Structural Mechanics & Heat Transfer Documentation (2013).

[12] G. Brunno, M. Kachanov. On modeling of microstresses and microcracking generated by cooling of polycrystalline porous ceramics. Journal of the European Ceramic Society 33, 1995–2005 (2013).

[13] M. de Jong, W. Chen, R. Notestine, K. Persson, G. Ceder, A. Jain, M. Asta, A. Gamst. A Statistical Learning Framework for Materials Science: Application to Elastic Moduli of k-nary Inorganic Polycrystalline Compounds. Scientific Reports 6, 34256 (2016).

[14] A. Jain, S.P. Ong, G. Hautier et al., Commentary: The Materials Project: A materials genome approach to accelerating materials innovation. APL materials 1.1 (2013).
[15] A. J. Cinthia, G. S. Priyanga, R. Rajeswarapalanichamy, K. Iyakutti, Journal of Physics and Chemistry of Solids, 79, 23-42, (2015).